J. Inst. Eng. India Ser. A (March 2020) 101(1):163–178
https://doi.org/10.1007/s40030-019-00418-3

ORIGINAL CONTRIBUTION

Stabilization of Expansive Clays by Combined Effects of Geopolymerization and Fiber Reinforcement

Mazhar Syed[1] · Anasua GuhaRay[1] · Sagar Agarwal[1] · Arkamitra Kar[1]

Received: 23 May 2019 / Accepted: 3 December 2019 / Published online: 10 December 2019

Abstract Expansive soil exhibits significantly low volumetric stability when exposed to moisture fluctuations, rendering it unsuitable for use in geotechnical applications. The present study emphasizes the stabilization of expansive black cotton soil (BCS) using envirosafe alkali-activated binders (AAB) with the inclusion of polypropylene (PP) fiber. AAB is produced by the reaction between an aluminosilicate precursor (Class F fly ash and/or slag) and an alkaline activator solution containing sodium silicate and sodium hydroxide. A water-to-solid (*w*/*s*) ratio of 0.4 is maintained for the AAB used in the present study. Physical, microstructural, and mineralogical characterizations for both untreated BCS and fiber-reinforced-AAB-treated BCS are performed through a stereomicroscope, X-ray diffraction, Fourier transform infrared spectroscopy, scanning electron microscope, energy-dispersive X-ray spectroscopy, and thermogravimetric analysis. The indirect tensile strength (ITS), swell/shrink test, California bearing ratio (CBR), and unconfined compressive strength for both untreated BCS and fiber-reinforced-AAB-treated BCS are carried out for different fly ash and GGBS (slag) proportions in the AAB mixture. The additions of varying percentages of fiber to AAB-treated BCS show a significant improvement in the geomechanical behavior of the soil. It is observed that the replacement of 5% of BCS mass by AAB prepared with 70% fly ash + 30% slag and containing 0.3% of PP fiber reduces the swelling pressure by 35–40%. The corresponding CBR and ITS values are found to increase by 40–45%. Recommendations for the practical implementation of fiber-reinforced AAB to treat BCS are provided based on the observations from this study.

Keywords Expansive soil · Alkali-activated binders · Polypropylene fiber · Microstructural characterization · Geotechnical characterization

Abbreviations

AAB	Alkali-activated binder
AS	Australian Standard
ASTM	American Society for Testing and Materials
BCS	Black cotton soil
BET	Brunauer–Emmett–Teller
BTCA	Butane tetracarbonic acid
C	Cohesion
CBR	California bearing ratio
CF	Coir fiber
CH	Heavy clay
CI	Intermediate plasticity
CL	Low plasticity
DTS	Direct tensile strength
e	Void ratio
EDS	Energy-dispersive X-ray spectroscopy
FP	Flexible pavement
FS	Flexure strength
FTIR	Fourier transform infrared spectroscopy
GGBS	Ground-granulated blast furnace slag
K.Br	Potassium bromide

✉ Anasua GuhaRay
anasua08@gmail.com

Mazhar Syed
p20170007@hyderabad.bits-pilani.ac.in

Sagar Agarwal
f20160447@hyderabad.bits-pilani.ac.in

Arkamitra Kar
arkamitra.kar@hyderabad.bits-pilani.ac.in

[1] Department of Civil Engineering, BITS-Pilani Hyderabad Campus, Secunderabad 500078, India

KOH	Potassium hydroxide
L.L	Liquid limit
Ls	Linear shrinkage
ITS	Indirect tensile strength
JSW	Jindal South West
MDD	Maximum dry density
NaOH	Sodium hydroxide
Na_2O	Sodium oxide
NTPC	National Thermal Power Plant
OMC	Optimum moisture content
PA	Pond ash
PET	Polyethylene terephthalate fiber
POFA	Palm oil fuel ash
PPF	Polypropylene fiber
PVA	Polyvinyl alcohol
PI	Plasticity index
PL	Plastic limit
pH	Potential of hydrogen
RHA	Rice husk ash
SEM	Scanning electron microscopy
SiO_2	Silicon dioxide
SL	Shrinkage limit
SSA	Specific surface area
STS	Split tensile strength
UCS	Unconfined compressive strength
USCS	Unified soil classification system
w/s	Water-to-solid ratio
XRD	X-ray diffraction
XRF	X-ray fluorescence
ϕ	Angle of internal friction

Introduction

Expansive black cotton soil (BCS) exhibits dual nature (swelling/shrinkage) when it is subjected to seasonal variation in moisture content. This is due to the presence of a high concentration of montmorillonite and smectite group in the soil which has a high affinity for water [1]. These volumetric changes can lead to extensive destruction of any structure constructed on them [2, 3]. As a result, stabilization using calcium-based binders like lime and cement has gained popularity to enhance the geotechnical properties of these expansive soils through hydration and pozzolanic reaction mechanisms. Sometimes, industrial wastes such as fly ash and slag are also used for these purposes [4, 5]. Utilization of envirosafe chemical binders is another modern approach for reinforcing weak expansive soils and shows a significant impact on their physicochemical and hydromechanical characteristics [6, 7]. Lime and cement are the most utilizable traditional binders for improving the bearing capacity and serviceability of soil in numerous structures such as foundation base, subgrade layer, and railway base [8]. However, the production of these traditional binders has some potential disadvantages and can lead to the emission of greenhouse gases like carbon dioxide (CO_2) and nitrous oxide (N_2O) [9, 10]. The usage of low-carbon-emission binders is an alternative to attain sustainability. It is encouraged to utilize the industrial wastes and by-products such as fly ash [5], ground-granulated blast furnace slag (GGBS), bagasse ash, pond ash, volcanic ash [11, 12], cement kiln, and marble dust [13], in combination with cementitious materials as binder to improve the geoengineering behavior of BCS. The inclusion of fibers and geotextiles further enhances the characteristics of these soils [14]. This technique aids to reduce the associated costs of dumping industrial wastes into landfills. Recently, the use of binders synthesized from alumina and silica-rich precursors for ground improvement by means of geopolymerization has attracted the attention of researchers [15]. Geopolymerization leads to the production of a long-chain polymeric sodium aluminosilicate compound upon the activation of fly ash and GGBS. A simple pozzolanic or supplementary cementitious reaction, however, using only slag and fly ash without alkaline activators will lead to the formation of a secondary or relatively weak calcium silicate hydrate matrix. This results in the development of poor mechanical strength and durability of the hardened cementitious paste. Alkali-activated binders prepared with both fly ash and GGBS are known to harden at a satisfactory rate under ambient conditions and provide satisfactorily high strength.

Incorporation of AAB using agro-waste and volcanic ashes to reinforce the soil is attempted by [6]. It has been found that the use of cementitious binders or AAB as additives in soil shows remarkable improvement in the compression and shearing resistance but behaves poorly against tensile loads. Consequently, to overcome the brittle nature of the soil, discrete polypropylene (PP) fibers are included in soil along with the binder-based additives [14]. Using only fly ash as precursor warrants thermal curing for desirable strength development and homogeneity of the reaction product formed. Also, the use of fly ash as the sole precursor delays the setting and eventual hardening of AAB. It has been reported in the previous studies that using slag along with fly ash results in high early- and later-age strengths without any significant requirement for thermal curing, thus resulting in a more energy-efficient binder. The main reasons for selecting AAB with polypropylene (PP) fiber are their negligible impact on the environment, producing significant bonding through friction, and their hydrophobic nature. The manufacturing process of AAB manufacturing does not produce any CO_2 emissions as it utilizes already available industrial wastes as raw

materials, as compared to Portland cement (PC) which emits 1 kg of CO_2 for each 1 kg of its production. Thus, the use of AAB in place of PC is not only useful in utilizing industrial waste but also useful in reducing CO_2 emissions. Polypropylene (PP) fibers consume less natural resources to be produced. They are biodegradable and widely recyclable. Burning of PP does not generate toxic gases like chlorine which is produced by the combustion of PVC. Hence, a combination of AAB and PP is a very eco-friendly arrangement. Moreover, these additives are cost-effective and possess the ability to control the swell-shrink potential and propagation of tensile cracks in the soil [16]. Several studies have proved the effectiveness of PP fibers in conjunction with cementitious binders in improving the geomechanical behavior of expansive soils. Table 1 provides a summary of research on PP fiber with different cementitious additives and their effects on geoengineering properties. However, limited studies are reported on the stabilization of soil using fly ash/slag-based AAB with a combination of PP fiber. Also, comprehensive research is required to investigate the tensile stiffness response of fiber–AAB-treated soil and thereby improve its ductile behavior.

Keeping the above issues in mind, the primary objective of the present study is to improve the geotechnical properties of expansive BCS using envirosafe AAB as an additive to soil. This study aims to overcome the brittle behavior of AAB-treated BCS by reinforcing it with short discrete PP fibers. A series of geotechnical characterization tests are conducted using different percentages of PP fiber with AAB. Microstructural characterizations are also carried out to understand the interfacial mechanism of fiber-reinforced AAB soil. This study also investigates the mechanical behavior of fiber-reinforced-AAB-treated BCS by varying the proportions of fly ash and GGBS in the AAB and proposes an optimum combination of fly ash and GGBS for the AAB to treat the BCS in practical applications. The materials used in this study are presented in the next section.

Materials

Black Cotton Soil (BCS)

BCS used in the present study is collected from Nalgonda region of Telangana state in India. It is dark brown in color and obtained from an open trench excavation of 300 mm depth in order to avoid the collection of vegetation or roots along with the soil. The soil is oven-dried before lumps are broken into small crumbs through wooden mallet. BCS is classified as high plasticity clay (CH) according to Unified Soil Classification System (USCS), and it is found to contain 78% clay. The specific surface area of BCS was obtained through the Brunauer–Emmett–Teller (BET) analyzer test, and it was found to be 249.28 m^2/g. The particle size distribution curves of raw BCS, along with fly ash and GGBS, are shown in Fig. 1. Tables 2 and 3 list the basic physical and engineering properties and the chemical composition of BCS, respectively.

Fly ash and Ground-Granulated Blast Furnace Slag (GGBS)

Fly ash used for this study is obtained from National Thermal Power Corporation (NTPC), Ramagundam City,

Table 1 Summary of research performed on soil stabilization using PP fiber with cementitious materials

Stabilization agents	Soil type	Effects	Optimum content	Remarks	References
Cement, FA with PPF	CL	UCS↑ Brittleness↓	8% cement, 30%FA, 1%PPF	–	[17]
Fly ash and CF	CI	LL, PI, MDD↓ UCS, CBR↑	20% fly ash, 1%CF	–	[18]
Cement with PPF	CL	Tangent modulus, UCS↑	0.2% PPF, 12% cement	Freeze–thaw cycle	[19]
Short PPF with PVA and BTCA solution	CH	Ductility, UCS↑, void ratio↓	1% PVA, 05% PPF, 1.5% BTCA	–	[20]
Fly ash with PET fiber	CL	Shear strength, CBR↑, PI↓	15% fly ash, 1.2% PET fiber	Subgrade for F.P	[21]
Marble dust with PPF	Soil	Tensile and compressive strength↑	10% marble dust with 0.5% PPF	–	[22]
POFA with Wollastonite fiber	Clayey soil	ITS, UCS↑	20% POFA, 5% W. fiber	NaOH, KOH solution	[23, 24]
Cement, GGBS with PPF	OH	UCS, STS, DTS, FS↑	75/25 cement and GGBS with PPF	–	[25, 26]
Cement with PPF and fiber bundles	Silty clay	UCS, ductility↑	8% cement, 0.5% PPF	Shanghai clay	[27, 28]
Cement with PPF	Soil	Interfacial mechanical strength↑	6% cement, 0.3% PPF	Bonding strength	[14, 29, 30]

↑ indicates increase, ↓ indicates decrease

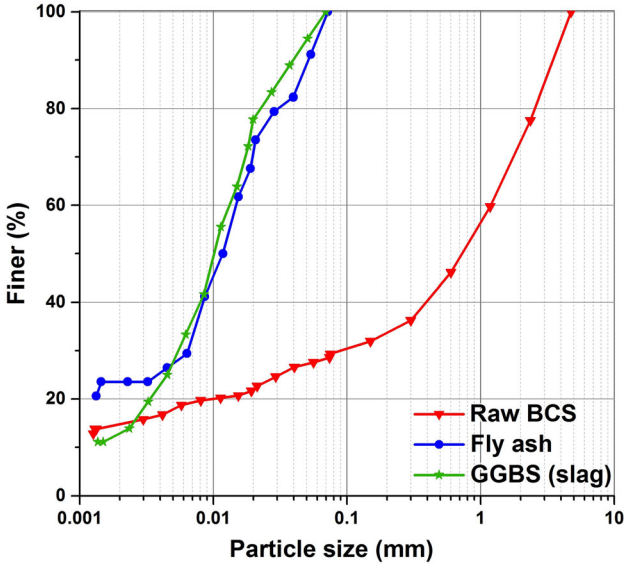

Fig. 1 Particle size distribution curves for BCS, fly ash, and GGBS

Table 2 Properties of raw BCS

Soil properties	Values
Soil classification (as per USCS)	CH
Specific gravity	2.58
Free swell Index, FSI (%)	88.30
Pore volume (cc/g)	0.047
Opt. moisture content, OMC (%)	24.0
Liquid limit, LL (%)	62.0
Shrinkage limit SL (%)	11.53
Plasticity index, PI (%)	38.0
Linear shrinkage, LS (%)	24.70
Activity	1.72
Max. dry density, MDD (g/cc)	1.65
Indirect tensile strength, ITS (kPa)	6.60
Un. compressive strength, UCS (kPa)	186
California bearing ratio	
Soaked	1.93
Unsoaked	5.58

Telangana, India. According to ASTM C618-17a, the fly ash is classified as Class F based on calcium, silica, alumina, and iron content in the ash. GGBS is collected from JSW Cement Ltd., Andhra Pradesh. The main oxide constituents of fly ash and GGBS are acquired through X-ray fluorescence technique (XRF), and their physical properties are presented in Tables 3 and 4.

Polypropylene Fiber (PPF)

Polypropylene (PP) fiber used in this study is supplied by Kankadurga Industries Pvt. Ltd., Hyderabad, India. The fiber length of 12 mm and a diameter of 0.033 mm are used in the present study. Figure 2 shows the physical appearance of PP fiber. The chemical properties of PP fiber are performed using X-ray fluorescence (XRF) technique and presented in Table 3. The physicomechanical properties of PP fiber are tabulated in Table 5 (datasheet supplied by the manufacturer).

Table 3 Chemical composition of raw materials

Elements	BCS	FA	GGBS	PPF
MgO	17.93	15.30	18.38	90.38
AL_2O_3	12.46	20.17	12.09	00.00
SiO_2	43.49	47.13	22.66	00.00
P_2O_5	01.27	01.24	00.00	01.37
SO_3	00.43	00.57	01.74	01.72
Cl	00.78	03.65	00.55	02.17
K_2O	03.76	02.55	00.60	00.57
CaO	08.97	03.11	40.65	02.46
TiO_2	01.34	02.00	01.23	00.17
MnO	00.15	00.10	00.94	00.00
Fe_2O_3	09.34	07.12	01.11	00.80
NiO	00.01	00.02	00.00	00.00

Table 4 Physical properties of FA and GGBS

Properties	FA	GGBS
pH	9.63	11.32
Specific gravity	1.92	2.72
Liquid limit (%)	19.4	–
Plasticity index (%)	NP	NP
FSI (%)	25	–
Loss of ignition	1.86	1.39
SSA (m^2/g)	0.74	0.36

Alkali-Activated Binder (AAB)

AAB is prepared by mixing the activator solution with dry aluminosilicate precursor (Class F fly ash and/or GGBS). The activator solution is prepared by blending the sodium hydroxide crushed pellets in sodium silicate solution with minimum water-to-solid (w/s) ratios. Both sodium silicate and sodium hydroxide chemicals are obtained from Hychem Chemicals Ltd., Hyd. Sodium silicate solution contains 14.7% Na_2O, 29.4% SiO_2, and 55.9% water. The activator solution is prepared a day prior to the usage. Hence, additional water along with these blends aids to reduce the residual heat and flash set. The mass ratio of sodium hydroxide to sodium silicate to fly ash/slag is 10.57:129.43:400 [31]. The percentages of fly ash and GGBS (slag) are also varied in the AAB mixture to obtain an optimum binder solution.

Fig. 2 Image showing discrete polypropylene fiber

Table 5 Basic engineering properties of PP fiber

Properties	Properties
Specific gravity	0.91
Tensile strength (MPa)	330
Young's modulus (MPa)	3500
Melting point (°C)	168
Burning point (°C)	585
Breaking tenacity (gpd)	4.4
Coefficient of friction	0.19
Water absorption (%)	0.03
Thermal and electrical conductivity	Low
Alkali and acid resistance	Good
Dispersibility	Excellent

Sample Preparation

Raw BCS is uniformly premixed with 5% of AAB paste (total dry mass of BCS) by maintaining a 0.4% w/s ratio in the alkaline binders before the mixing of PP fiber. From the previous study, it is observed that 5% AAB in BCS shows rapid gain in shear strength, good workability, excellent binding properties, low alkali reactivity, and lower greenhouse gases emission and is also economical compared to other proportions. Hence, 5% AAB is proposed as an optimum binder content in the present study [32]. Selected AAB mixes with varying fly ash, and slag proportions are manually compacted in a mold with dimensions 950 × 480 × 150 mm. The compaction is performed using a 9-kg steel rammer with free fall height of 310 mm in three layers. This procedure of compaction is replicated for all six different AAB mixes with varying fly ash and slag proportions. The prepared specimens are cured using moist jute bags to ensure uninterrupted and uniform curing for 24 h. Prior to random mixing of different percentages of PP fiber (0%, 0.10%, 0.20%, 0.25%, 0.30%, and 0.4% by weight of BCS) in the AAB-blended soil, it is oven-dried. A series of geoengineering and microscopic analysis are performed to investigate the effect of fiber and AAB blend on the geomechanical behaviors of the composite samples. Table 6 provides the nomenclature of different types of samples prepared. The fiber–AAB-treated soil specimens are designated as $S.A_5$ $(F_xG_y)P_z$ where S denotes black cotton soil, A_5 denotes 5% of AAB (5% total mass of BCS), F denotes fly ash, and the subscript x denotes fly ash content in the AAB mixture, G denotes GGBS, and the subscript y denotes GGBS content in the AAB mixture, P denotes the polypropylene fiber, and the subscript Z denotes the mass percentage of polypropylene fiber.

Experimental Methodology

Chemical Characterization

X-Ray Diffraction (XRD)

X-ray diffraction analyses are performed using a Rigaku Ultima-IV diffractometer to identify the minerals present in the untreated and AAB-treated BCS. Dry powder soil samples are inspected through CuKα rays produced at 40 mA and 40 kV with an operating 2θ range from 0° to 80° at 0.02° 2θ steps and integrated at 2 s. per step.

Fourier Transform Infrared (FTIR) Spectroscopy

Fourier transform infrared (FTIR) spectroscopy is conducted to characterize the various molecular bonds present in both treated and untreated BCS using a JASCO FTIR 4200 setup through KBr pellet arrangement. The transmittance spectral range is chosen from 4000 to 500 cm^{-1} for all the samples.

Table 6 AAB solution preparation ratios with fiber and sample definitions

Combination	Sample definition
Combined percentage of fly ash and slag (GGBS) were kept as 100%	$S.A_5\ (F_xG_y)P_z$
Mixing of 5% AAB paste (total mass of soil) into the BCS	S = BCS; A_5 = 5% of AAB; F = fly ash; G = GGBS(slag);
fiber–AAB-treated soil cured for 24 h before testing.	$x + y = 100$, x = fly ash content in the AAB mixture; y = Percentages of GGBS in the AAB mixture (0, 10, 20, 30, and 40); P = polypropylene fiber; z = fiber content (0%, 0.10%, 0.20%, 0.30%, and 0.40% of BCS)
	$S.A_5\ (F_{100}G_0)P_{0.3}$; $S.A_5\ (F_{90}G_{10})P_{0.3}$;
	$S.A_5\ (F_{80}G_{20})P_{0.3}$; $S.A_5\ (F_{70}G_{30})P_{0.3}$; and
	$S.A_5\ (F_{60}G_{40})P_{0.3}$; similarly for other fiber content

Stereomicroscopy Imaging

Stereomicroscopic images are used to visualize the surface texture and physical features of untreated BCS, as well as fiber–AAB-treated BCS using an Olympus SXZ7 setup with the least dimension of 20 μm. Images are captured at various magnifications to relate the characteristics of PP fiber, before and after AAB immersion in the BCS. The target region is selected indiscriminately of all samples.

Scanning Electron Microscope (SEM) and Energy-Dispersive X-ray Spectroscopy (EDS)

Scanning electron microscopy (SEM) is conducted using an Apreo setup provided by FEI (Field Electron and Ion Company) at different magnifications. Surface morphology and elemental composition are examined for both untreated and fiber–AAB-treated soil at various spot regions. 20 kV excitation voltages are maintained throughout the study in order to avoid the electron cloud and blurred condition of images. Energy-dispersive X-ray spectra (EDS) are recorded through the Aztec analyzer system provided by Oxford Instruments with a probe current of 65.4–67.0 μA at a working distance of 10 mm.

Thermogravimetric Analysis (TGA)

Differential thermogravimetric analysis (TGA) is performed using Shimadzu/DTG-60 setup at a heating rate of 10 °C/min for a mass sample of about 15 mg up to 500 °C under nitrogen-rich atmosphere. Thermal stability analysis of both untreated and fiber–AAB-treated BCS is examined at different elevated temperatures.

Geoengineering Characterization Tests

A series of geomechanical tests are performed for both untreated BCS and AAB-treated soil at different PP fiber contents. All the soil specimens are prepared at their MDD and OMC values. These results are used to assess the effectiveness of stabilizers which aid to control the drastic volume change.

Basic Geotechnical Characterization

Basic geotechnical characterization tests such as compaction, Atterberg's limits, and free swell index are carried out for each of the cases mentioned in Table 7 following IS 2720-8 (1983), IS 2720-5 (1985), and IS 878 (1956) codes, respectively.

Linear Shrinkage

The shrinkage characteristics of BCS amended with varying percentages of PPF are carried out as per the Australian standard code (AS 1289.C4.1-1977). Semi-cylindrical shrinkage molds of length 140 mm with radius 12.5 mm and height of 20 mm are completely filled with wet soil. The specimen is first maintained at room temperature for 24 h and then transferred into the oven for 24 h at 110° C. The linear shrinkage L_S (%) is given by

Table 7 Basic engineering tests of AAB-treated soil with varying content of fly ash and GGBS

Properties	$S.A_5\ (F_{100}G_0)$	$S.A_5\ (F_{90}G_{10})$	$S.A_5\ (F_{80}G_{20})$	$S.A_5\ (F_{70}G_{30})$	$S.A_5\ (F_{60}G_{40})$
MDD (g/cc)	1.78	1.82	1.87	1.91	1.89
OMC (%)	18.9	19.3	19.1	18.8	19.0
FSI (%)	38.0	37.0	35.0	31.0	28.0
LL (%)	33.8	32.6	31.7	30.1	29.5
PI (%)	21.8	20.9	20.2	19.1	19.6

$$L_S = \frac{L_i - L_f}{L_i} * 100$$

L_i is the initial length of soil; L_f is the final length of soil.

Consolidation and Swelling Pressure

One-dimensional consolidation tests are performed in an oedometer apparatus according to ASTM D-2435. Both untreated BCS and fiber–AAB-treated BCS samples are statically compacted in a consolidation ring of 20 mm thickness and 60 mm diameter. The sample is sandwiched between two porous stones and two filter papers. After the equilibrium, the samples are subjected to compression by load increment at every 24 h. The e-log (p) curve is obtained from the results of the experiment.

One-dimensional swelling pressure tests are conducted using a constant volume method as per ASTM D-4546. Soil specimens are molded in a consolidation ring of 20 mm thickness and 60 mm diameter at a maximum dry density of soil. After assembling the sample between the porous stones, it is mounted centrally on the top of the porous stone to the loading block of proving ring. The change in dial gauge and proving ring readings are noted at different intervals of time. In order to maintain a constant volume of the specimen, the plate is adjusted in such a manner that the dial gauge always shows the original reading.

Unconfined Compressive Strength (UCS)

Undrained shear strength tests are performed on the specimens using strain-controlled application of static load in accordance with ASTM D-2166. Untreated BCS and AAB-treated BCS samples are shaped in a cylindrical mold length of 76 mm with an inner diameter of 38 mm at MDD-OMC. Samples are stored in an airtight vacuum desiccator for maturation. A strain rate of 1.2 mm/min is used during loading.

Indirect Tensile Strength (ITS)

The indirect tensile test is conducted as per ASTM D4123-1995 standard by using the Marshall Stability Machine by attaching a loading strip of 12.5 mm on the load frame (Fig. 3). Soil samples are compacted with respect to their moisture content and dry density (shown in Table 7), in a cylindrical shape of 100 mm diameter and 80 mm height. Specimens are preserved for a minimum of 24 h in the humidity chamber prior to loading. The test specimens are loaded at the rate of 50.5 mm/min through the steel loading strip-till failure. The tensile strength S_t in mPa is given by

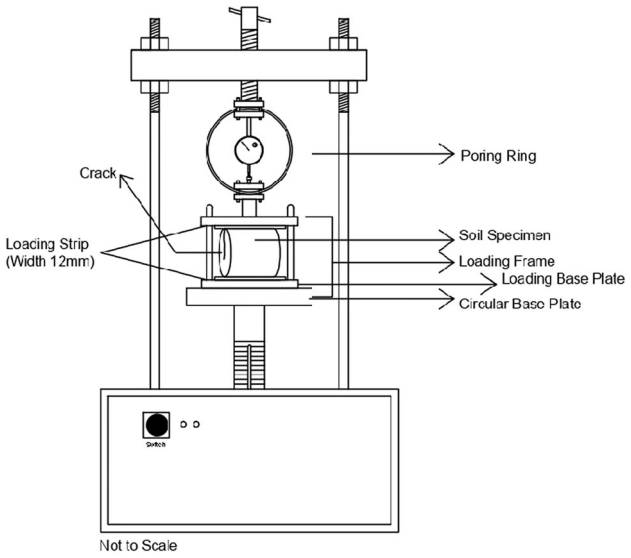

Fig. 3 Schematic diagram of indirect tensile test

$$S_t = \frac{2P_{ult}}{\Pi td}$$

P_{ult} = ultimate load at which failure of sample occurred in (N), t = thickness of specimen (mm), and d = diameter of the specimen (mm).

California Bearing Ratio (CBR)

Soaked CBR test is performed for different compositions of AAB and fiber content in the BCS using ASTM D-1883. Fly ash/GGBS-based AAB-treated BCS specimens are prepared with their MDD-OMC values which are tabulated in Table 7. It measures the stiffness of a subgrade layer by soaking the specimen for 96 h in water prior to testing with a static strain rate of 1.25 mm/min through a loading frame of 50-mm-diameter plunger.

The results obtained from these experiments are discussed in the next section.

Results and Discussion

Chemical Characterization

XRD

XRD is an intrinsic technique to analyze the crystalline compounds in clay mineralogy. Figure 4 shows the powdered XRD patterns of both untreated BCS and AAB-treated BCS with varying percentages of fly ash and GGBS in the AAB mixture. The dominant clay mineral present in the untreated BCS is montmorillonite (M), indicated by the peaks observed at 2θ values of 19.7°, 28.1°, 36.6°, and

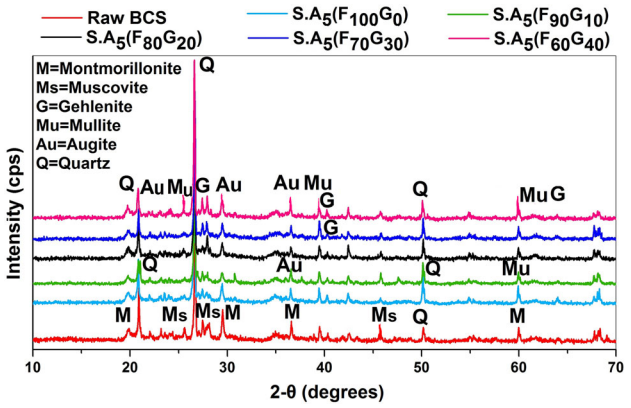

Fig. 4 XRD pattern of untreated BCS and fly ash/slag-based AAB-treated BCS

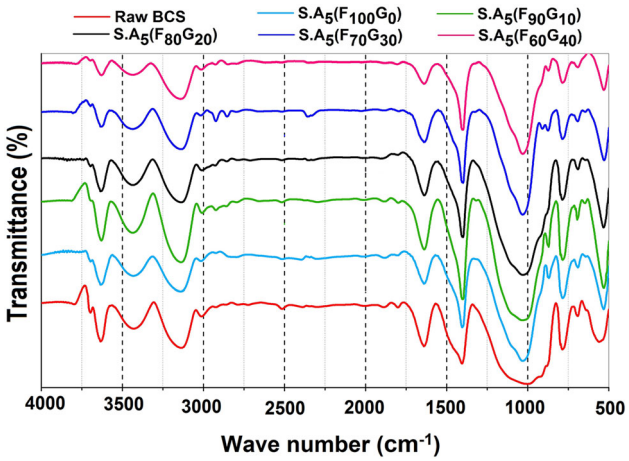

Fig. 5 FTIR spectroscopy of untreated BCS and fly ash/slag AAB-treated BCS

61.8°. A small amount of quartz (Q) at 2θ values of 21.9°, 26.8°, and 50° is also observed. Other reflections correspond to muscovite (Ms) at 2θ values of 23.4°, 27.6°, and 45.4°. After the addition of AAB to the BCS, some noticeable changes take place in the mineralogy, as evident from the diffractograms. It is observed that there is a significant reduction in the peak intensities corresponding to montmorillonite (M). This can be attributed to the alteration in the chemical composition of the clay minerals [3]. As expected, the sharp crystalline peaks of Quartz (Q) remain the same. Moreover, the XRD patterns of all treated specimens reveal additional peaks corresponding to mullite (Mu) near the 2θ values of 27.3°, 36.1°, and 61° and augite (A) at 27.1°, 29.6°, and 36.3°, respectively. These minerals roughly correspond to the crystalline phases present in hardened AAB paste [10]. It is also interesting to note that with an increase in the amount of GGBS in the AAB mixtures, additional peaks corresponding to gehlenite (G) show up at 2θ values of 27.9°, 39.1°, and 62.2°. The formation of this mineral can be attributed to the geopolymerization reaction of the AAB. Flatter portions of the diffractogram indicate amorphous phases of the pozzolanic additives and the clayey particles. Hence, it can be concluded that the fibers and the AAB remained in conjunction with BCS after forming the blends that render the improvements in the mechanical properties. FTIR spectroscopic analyses are performed to supplement the observations from the XRD analyses. The results are presented in the next section.

FTIR Spectroscopy

Figure 5 shows the transmittance spectra of BCS before and after using AAB treatment with varying proportions of fly ash and GGBS in the AAB additives. The spectrum curve of raw BCS shows general characteristics of montmorillonite with a sharp peak around 3660 cm^{-1} for -OH stretching group. After AAB treatment, there is a slight reduction in the intensity of chemical bonds corresponding to montmorillonite in the BCS. This decrement is due to weathering action on clay surfaces [12]. Furthermore, the broad bands are found at 3616 cm^{-1} and 3450 cm^{-1}, corresponding to the O–H stretching in Portlandite [$Ca(OH)_2$] of a structural hydroxyl group and water [6]. For all selected samples, the C–H methyl and methylene groups may represent around 2950 cm^{-1}. The presence of C=O carbonyl bond is detected at 1730 cm^{-1}. However, the peaks correspond to bending vibration of the $=CH_2$ group observed at 1460 cm^{-1}. The appearance of the transmittance peak around 1450 cm^{-1} indicates that the cellulose and hemicellulose might have expelled due to the AAB inclusion [31]. Another main peak ranging from 1004 to 1033 cm^{-1} is attributed to Si–O–Si antisymmetric stretching. In addition, a new molecular bond can be observed around 910 cm^{-1} which corresponds to Al–OH stretching vibration on the fiber–AAB-treated BCS. Other relatively significant bands appeared in the regions 770, 690, and 530 cm^{-1} which represent the spectra corresponding to the stretching and bending of Si–O–Al group. Similar bonds are visible for both untreated BCS and fiber–AAB-treated BCS but most of them show chemical shifts, indicating impermeable nature of BCS due to the geopolymeric reaction between the pozzolanic materials and alkali activator [10].

Stereomicroscopy Imaging

Figure 6a–d displays the typical surface images for both untreated BCS and fiber–AAB-treated BCS. Figure 6a shows the untreated BCS which consists of yellowish and light reddish-colored particles indicating the presence of iron in the oxidized condition. Some dark brown regions

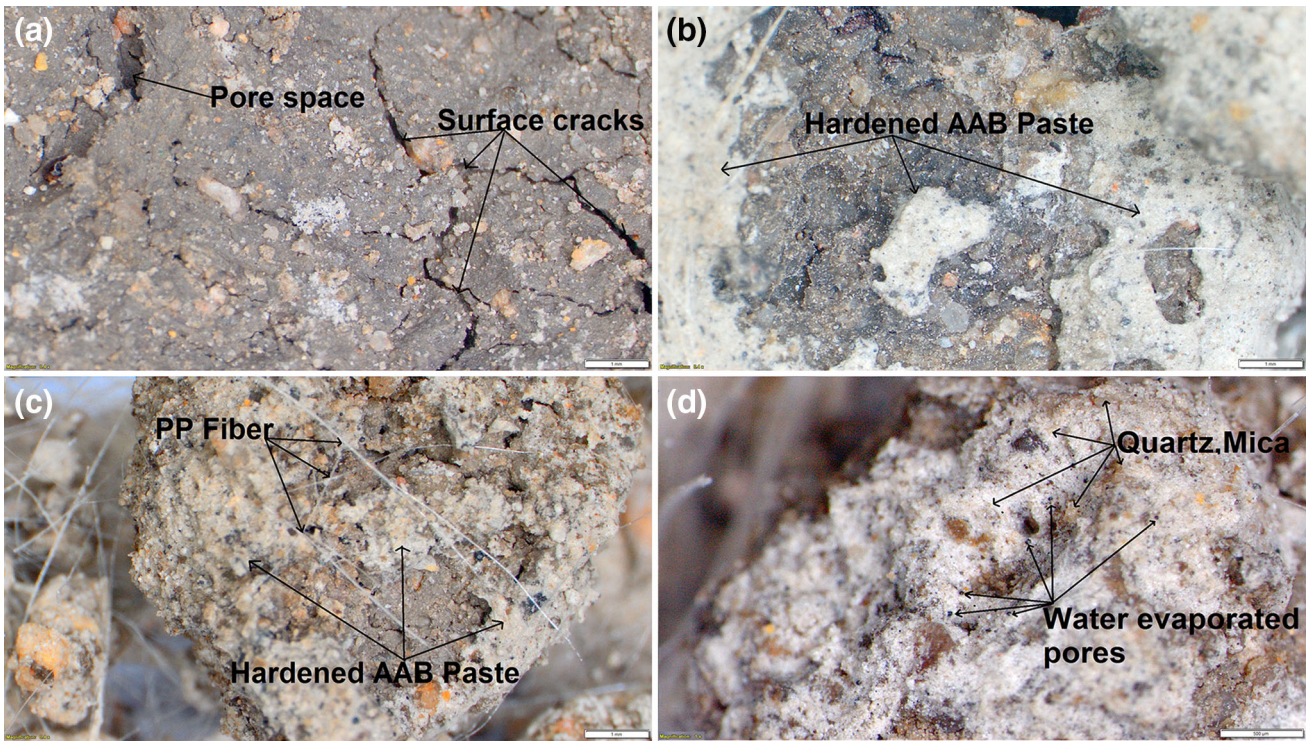

Fig. 6 Stereomicroscopy images of **a** untreated BCS, **b** AAB-treated BCS, **c** fiber-reinforced AAB-treated BCS, **d** combination of fly ash/slag-based AAB-treated BCS

reveal the presence of illite and smectite group which tends to be highly organic soil. The montmorillonite mineral tone of clay is generally associated with the presence of iron and manganese composites [33]. There are also some visible surface cracks on untreated BCS, which have effects on the swelling and shear strength properties. Figure 6b shows a deposit of hardened AAB paste around the clay interface which aids to fill the pores and cracks by forming a thin layer of hardened AAB paste. Figure 6c shows discrete fiber–AAB layer around BCS which enhances tensile strength. The fiber–AAB inclusions in BCS act as a bridge surface by holding the clay particles strongly around the fiber. The bright and shiny regions in Fig. 6d exhibit mica from the pozzolanic materials, and dark black-colored patches reflect the voids by water evaporation from the hardened AAB mixture due to highly exothermic geopolymerization reaction between the clay particles and aluminosilicate precursors [34]. In addition, the grayish color along with the shiny region of sodium aluminum silicate hydrate in the AAB paste represents the quartz formation. Thus, the fiber surface is partially covered with clay particles that reduce the brittleness behavior, forming the unitary matrix.

XRD and FTIR provide qualitative information regarding the chemical composition of the materials. Stereomicroscopy too provides qualitative information regarding the physical characteristics of the materials. In order to obtain quantitative information, SEM in conjunction with EDS analyses is performed as shown in the next section.

Scanning Electron Microscope (SEM) and Energy-Dispersive X-Ray Spectroscopy (EDS)

Micrographs of AAB-treated and fiber-reinforced BCS are presented in Fig. 7a–d. Figure 7a shows that the smooth spherical surfaces varying from small to large particles and represent the unreacted fly ash in the BCS. However, numerous elongated spindle shapes are closely bounded with fly ash particles through sodium aluminosilicate gel around the irregular aggregated clayey surfaces. It is observed from Fig. 7b that a discrete soil matrix covered with slag and fly ash in the form of reticulated circular structure. This drastic change in surface morphology is attributed to the formation of the flocculated network with more cementitious structure [35]. EDS provides the weight percent of elements present in BCS. As expected, carbon (C) and oxygen (O) are found to be the significant components of the AAB-treated soil. With the replacement of fly ash by GGBS in the AAB mixture, the residual fly ash textures start bonding with clay particles and form a pitted gel matrix structures as shown in Fig. 7c. It was also noted that the presence of slag in the BCS can produce an early bonding agent between the soil surface layers in the form of spherical vitreous gel [33]. These cementitious gel

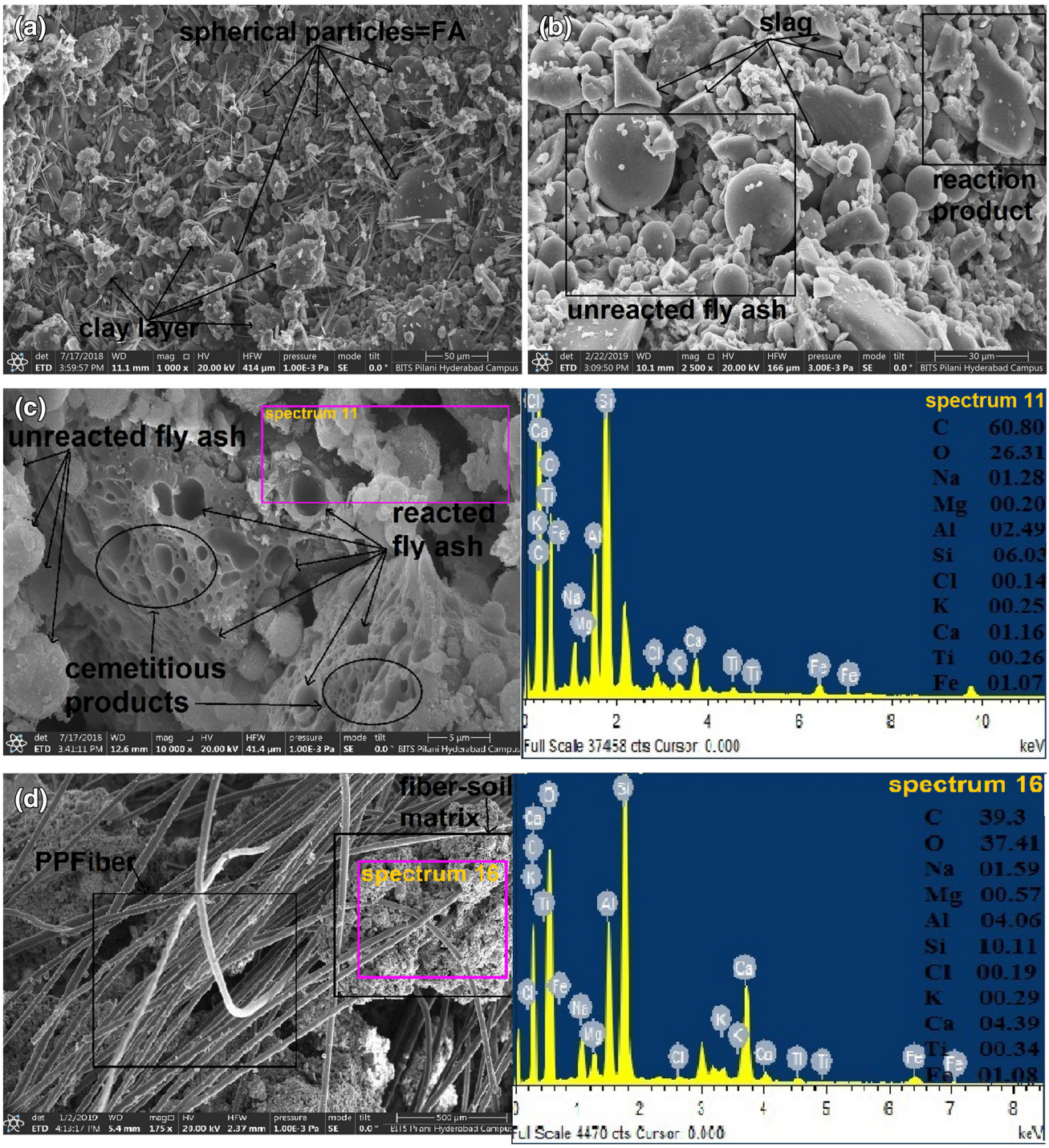

Fig. 7 SEM/EDS images of **a** 100% fly ash-based AAB-treated BCS, **b** 70% fly ash/30% slag-based AAB-treated BCS, **c** elemental analysis for reacted fly ash AAB BCS, **d** fiber inclusion in AAB-treated BCS

accretions may be attributed to the formation of geopolymerization. Thus, the accumulation of calcium silica aluminum hydrates and cementitious products leads to the reduction of voids and pore spaces between the clay particles [12]. Figure 7d shows the series of discrete fiber bounded with pozzolanic material in the clay minerals which makes the contribution to improving bond strength. The inclusions of fiber act as a spatial thread groove network to interlock the clayey particles by reinforcing the tensile properties. Peak intensities of calcium (Ca), silica (Si), alumina (Al), and oxygen (O) become relatively stronger with the replacement of fly ash with GGBS in the fiber-reinforced-AAB-treated BCS. The percentage of calcium increases with the increase in GGBS content in the

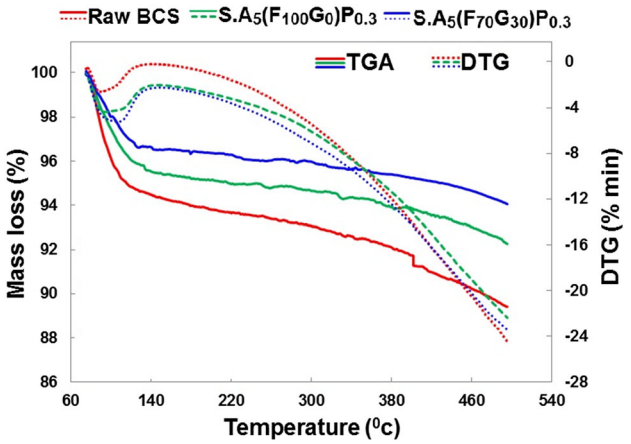

Fig. 8 TGA/DTG curves of untreated BCS and AAB-treated BCS

AAB mixture. Thus, the improvement in shear strength properties of fiber–AAB-treated BCS is mainly due to pozzolanic reaction [25].

To confirm the findings from the SEM–EDS analyses, TGA and DTG analyses are performed.

Thermogravimetric analysis (TGA)

Thermogravimetric (TG) and derivative thermogravimetric (DTG) curves for the untreated BCS and 5% AAB-treated BCS with polypropylene fiber at different proportions of fly ash and GGBS in the AAB mixture are presented in Fig. 8. As the temperature increases, various substances in the soil sample start decomposing, leading to a loss in mass at the respective temperature. The TG curves for both untreated BCS and fiber–AAB-treated BCS samples indicate an initial loss in mass around 140 °C due to vaporization of hygroscopic and adsorbed water [4]. As can be seen from Fig. 7, the percentage of mass loss is high for untreated BCS (5–6%) when compared to AAB-treated BCS (3–4%). This reduction in dehydration peaks may be attributed to the geopolymerization reaction between the clay and pozzolanic compounds [12, 36]. In addition, a minimal loss in mass is observed around 330 °C due to the destruction of crystalline structure in the BCS. Furthermore, the TGA curves follow asymptotic behavior beyond 600 °C. Hence, the fiber–AAB treatment contributes to rearrange the montmorillonite octahedral structure in the clay surfaces.

Geoengineering Characterization

Basic Geotechnical Characterization

Table 7 shows the basic geoengineering tests of AAB-treated BCS with varying content of fly ash and GGBS in the AAB mixture. It can be observed from Table 7 that the addition of GGBS in place of fly ash does not have any significant effect on the plasticity of the soil-AAB mixture. However, the OMC and MDD values are increased with increased slag content in the AAB compound. In addition, the free swell index reduces by approximately 25% for $S.A_5$ ($F_{60}G_{40}$). This reduction may be attributed to the formation of multivalent cations and flocculation structure [4, 5]. The subsequent decrease in the specific surface area and water affinity of clay particles results in a reduction of plasticity and swell–shrink properties. The addition of AAB in the BCS leads to reduce the liquidity characteristics mainly because of encapsulation of clay particles through geopolymerization. As the replacement of fly ash with slag increases in the soil-AAB mixture, the plastic and shrinkage property of soil gradually increases. Moreover, the addition of fiber is beneficial to BCS, as it controls the shrinkage and brittleness behavior upon the addition of GGBS in the soil.

Linear Shrinkage

The linear shrinkage results for both untreated BCS and AAB-treated BCS with varying content of fly ash and GGBS in the fiber–AAB mixture are shown in Fig. 9. The shrinkage limit and linear shrinkage of raw BCS are found approximately 11.53% and 24.6%, respectively, indicating high shrinkage [37, 38]. Cornell University (1951) has classified the Atterberg's limit based on clay minerals and exchangeable ions. ASTM D-121 also classified the relative expansivity of the soil swelling based on consistency parameters, especially shrinkage limit. Particle size and mineral composition are the primary functions for causing

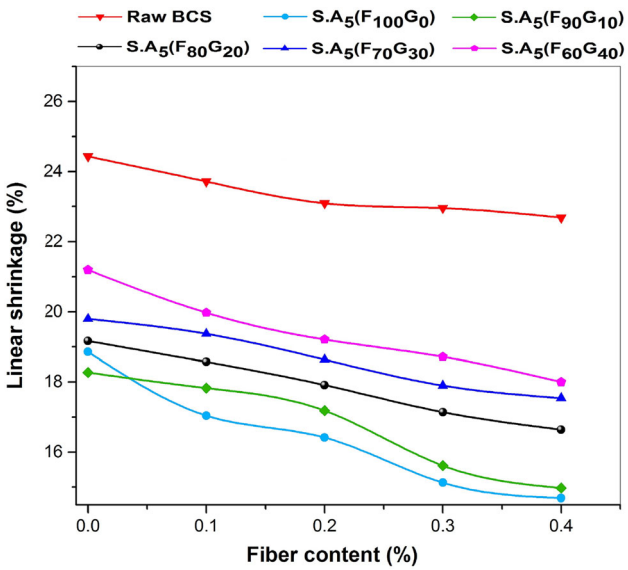

Fig. 9 Variations of linear shrinkages of fiber-reinforced BCS with varying content of fly ash and GGBS

high shrinkage and swelling in soil. BCS is rich in montmorillonite and smectite group of clay minerals which has tendency to hold high moisture, influencing low volumetric stability upon wet and dry cycles. The inclusion of fly ash-based AAB additive in the BCS leads to reduce the linear shrinkage values from 24.4 to 14.6%. This decrement may be attributed to the formation of pozzolanic phenomena around the clay surfaces [39]. As a result, the surface area of clayey particles decreases and plasticity decreases. Further addition of fiber in AAB-modified BCS shows a marginal effect on linear shrinkage and controls the cracks. Thus, the significant improvement of linear shrinkage can be due to the development of strong interaction between fiber surface and AAB soil matrix. As the replacement of fly ash with GGBS content increases in the AAB mixture, the shrinkage behavior also increases. This enhancement may be induced due to low liquidity and capillary forces by accelerating the pozzolanic reaction [40]. Moreover, it is interesting to note that the 100% fly ash content in the fiber–AAB paste shows the highest decrement in linear shrinkage percentages, which indirectly diminishes the plasticity index [5, 11]. Hence, the combination of fly ash-based AAB and fibers shows low shrinkage than the fly ash-/GGBS-based AAB-reinforced soil.

Consolidation and Swell Pressure

The compressibility behavior of untreated BCS and fiber–AAB-treated BCS with varying fly ash and GGBS is represented by the slope of void ratio versus logarithmic stress (e-log p) curve in Fig. 10a. The initial void ratio is found to be the highest for the raw BCS (0.923). However, the equilibrium void ratio decreases from 0.908 to 0.48 when the BCS specimens are blended with varying fly ash and GGBS content in the fiber–AAB mixture, and the significant reduction of the void ratio can be attributed toward the formation of a strong interlocking particle and new mineralogy [41]. Furthermore, as the GGBS content increases in the AAB compound, the final settlement and the structural gaps in mineral skeleton also decrease further [42–44]. It can be observed from the consolidation curves that the equilibrium void ratio of modified soil replaced with 0, 10, 20, 30, and 40% of fly ash with GGBS in the fiber–AAB mixture are about 0.681, 0.652, 0.600, 0.587, and 0.562, respectively. The intention of adding GGBS in the AAB mixture is to enhance the rate of geopolymerization reaction between the sodium aluminosilicate and clayey particles [10]. The main mechanisms that govern the deduction in e-log p curves of all modified soils are physicochemical forces (interlocking density, suction, and cation exchange), morphological changes (pozzolanic reaction, flocculation, and mineralogical alteration), and calcium-based aluminosilicate gel formation.

Figure 10b shows the variation of swelling pressure curves for both fiber–AAB-reinforced BCS and untreated BCS. It can be seen from time–swell curves that the raw BCS takes maximum time to attain the equilibrium swelling pressure. The result indicates that the swelling property of all modified soil drastically reduces even with a small inclusion of an alkali activator solution of sodium hydroxide and sodium silicate with the synthesis of aluminosilicate precursor. Although the addition of fly ash alone in the alkaline binder causes an insignificant reduction in swelling potential and heave characteristics of expansive soil, this reduction could be attributed to the effect of high interlocking particle density and pozzolanic reaction induced between the clay particles [27, 45]. Subsequently, as the replacement of fly ash with GGBS increases in the fiber–AAB mixture, the rate of swelling pressure and compressibility of soil significantly decreases. It is interesting to note that the incorporation of 30% GGBS and 70% fly ash in the AAB mixture to BCS generates least

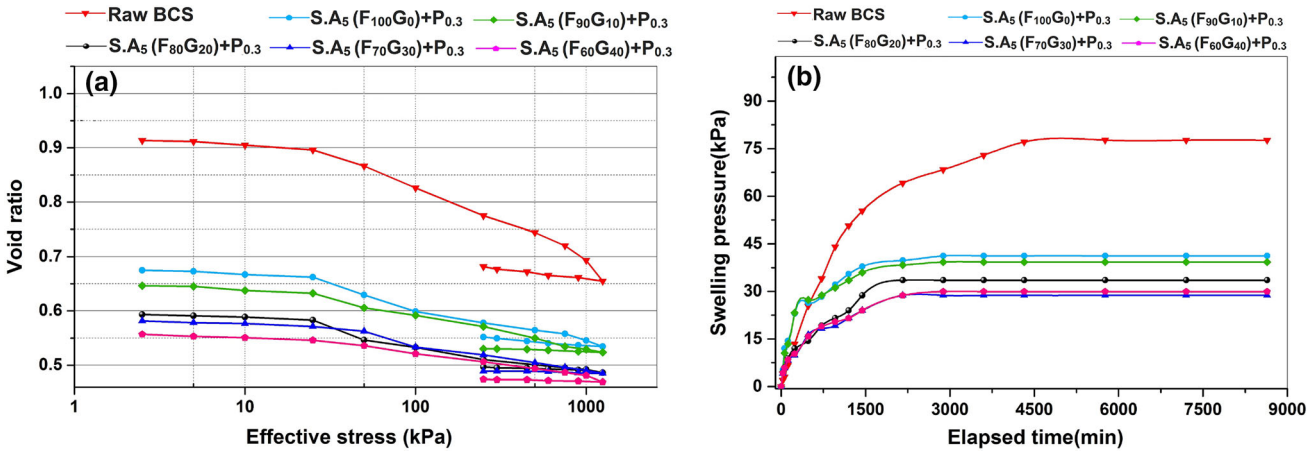

Fig. 10 Variations of **a** e-log (p) curves, **b** swelling pressure of untreated BCS and fiber–AAB-treated BCS at varying fly ash and GGBS content

swelling pressure among all proportions of fly ash/slag-based AAB-reinforced soil. The inclusion of 5% AAB in the BCS alters the clay mineralogy by dissolutions of clayey particles with pozzolanic additives [46]. This reaction may lead to minimize the plasticity characteristics and swelling potential. As the GGBS content increases in the AAB mixture, the swelling pressure and void ratio of BCS decrease significantly. GGBS with water leads to produce silicate hydrates (CSH) from its available calcium and silica causing less moisture attraction in soil. The addition of fiber does not alter much on swelling behavior. The reduction in swelling and compressibility of soil is majorly from pozzolanic integration and dissolution of particles by altering clay mineralogy.

Unconfined Compressive Strength (UCS)

The compressive shear strength of untreated BCS and aluminosilicate precursor-based AAB-treated BCS at varying content of fiber is shown in Fig. 11a. A negligible improvement in UCS is observed between raw and fiber-reinforced BCS samples. From the results, it is also noticed that the combined addition of fly ash and GGBS in the fiber–AAB mixture shows relatively higher compressive strength. Although the replacement of 30% fly ash with GGBS in the AAB mixture achieves maximum shear strength compared to all other stabilized soil, the influence of fiber with AAB causes the interfacial friction between the fiber and soil matrix which exhibits more ductile behavior and stretching resistance [14]. In addition, a minimal reduction in undrained shear strength is also observed due to a higher dosage of fiber content (beyond 0.3%) of all treated soil specimens. This reduction may be attributed to the formation of smooth texture fiber [47]. Results on stress–strain response are presented in Fig. 11b for various content of fly ash and GGBS in the AAB mixture with 0.3% of fiber inclusion. It can be seen from Fig. 11b that raw BCS shows the low peak stress at the strain of around 2.3%, indicating a weak shear strength property, while the fiber–AAB-treated BCS shows the drastic improvement in compressive strength at low strain. This abrupt enhancement can be because of geopolymeric reaction induced between the sodium aluminosilicate and pozzolanic additives in the clay particles [48]. It is interesting to note that the shear stresses increase with increasing the fiber and GGBS content in the blended compounds. The increase in mechanical strength is mainly due to the confinement bonding and frictional resistance of the fiber during shear.

Indirect Tensile Strength (ITS)

The variations of tensile strength values for both untreated BCS and AAB-treated BCS with different fiber contents are shown in Fig. 12a. The trend of ITS values with an increasing amount of fiber content in the raw BCS shows marginal improvement from 7.5 to 14.8 kPa, respectively. It can be seen from Fig. 12a that the tensile strength of all AAB-treated soil increases with increasing fiber content. The inclusion of fiber–AAB compound in the clay matrix aids to reduce the deformation and brittleness behavior [30]. Furthermore, as the replacement of fly ash with GGBS increases in the AAB mixture, the formation of cementitious compounds and interfacial bonding behavior between the soil and fiber increases [21]. A vigorous increment is observed in the tensile peak of BCS stabilized with 70% fly ash and 30% GGBS in the 5% AAB mixture. Thus, the enhancement in ductile behavior of modified

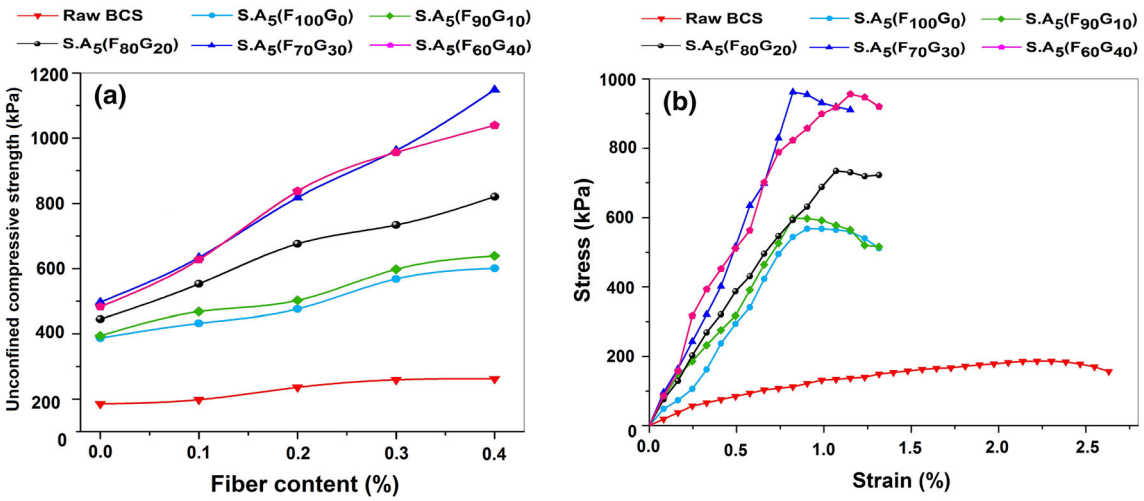

Fig. 11 Variations of **a** UCS of fiber–AAB-reinforced BCS, **b** stress–strain curves of untreated BCS and fiber–AAB-treated BCS at different combinations of fly ash and GGBS

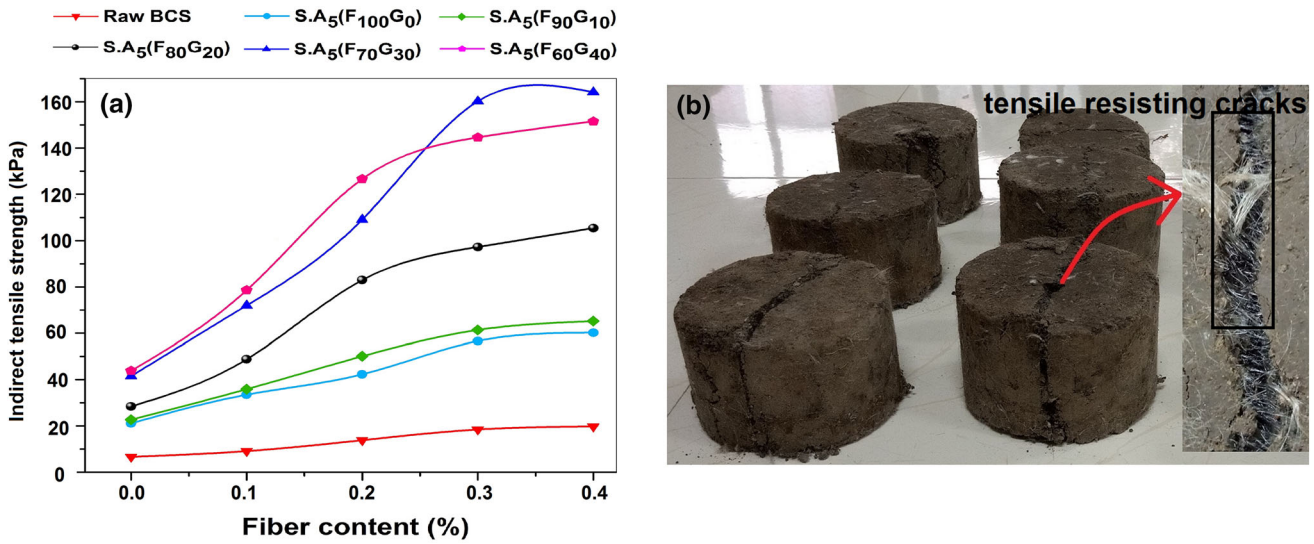

Fig. 12 Variations of **a** ITS of fiber-reinforced BCS with varying content of fly ash and GGBS, **b** effect of fiber on tensile resistance of AAB-treated BCS

BCS can be achieved through friction and particle bonding [26]. The addition of 0.3% polypropylene fiber to AAB-treated soil can effectively control the formation of tensile cracks and sliding properties; this, in turn, leads to greater tensile resistance and transform from brittle to ductile behavior through optimum interfacial surface interaction between clay and fiber matrix. It is also interesting to note that the ITS values of all AAB-treated soil is not greatly enhanced at 0.4% fiber inclusion when compared to 0.3% of fiber. These minimal changes are due to the formation of smooth texture fiber and weak bonds between the soil/fiber interactions [47]. Figure 12b shows the tensile failure of fiber–AAB-treated soil, and the failure pattern shows the tensile cracks between the particles.

California Bearing Ratio (CBR)

The results of the soaked CBR test on both untreated BCS and fiber–AAB-treated BCS with a different combination of fly ash and GGBS in the AAB compounds are presented in Fig. 13. Observations are taken between the test load (penetration resistance) versus the penetration of plunger at 2.5 and 5 mm, respectively. The soaked and unsoaked CBR value of raw BCS is found approximately 1.96 and 5.02% at 2.5 mm of penetration, indicating low strength bearing. As seen from graph that the inclusions of 100% fly ash-based geopolymeric AAB mixture along with fiber increases the soaked CBR value from 1.96 to 4.89%, respectively. The drastic improvement in strength bearing ratio may be attributed toward the pozzolanic reactions that catalyze the properties of fly ash and GGBS during the period of soaking [11]. As the inclusion of fiber and GGBS content increases in the AAB-treated soil, the CBR values

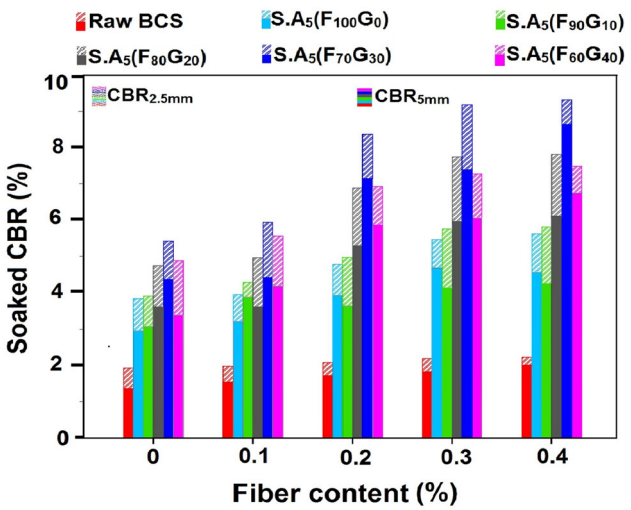

Fig. 13 Comparison of soaked CBR values at 2.5 mm and 5 mm penetrations of AAB-treated BCS with varying percentages of fiber

are also found to increase. In addition, the highest soaked CBR value is found at 0.3% polypropylene fiber with 30% replacement of fly ash with GGBS in the 5% AAB paste. The addition of GGBS in the fiber–AAB-treated soil aids to enhance the rate of geopolymerization reaction and alters the montmorillonite morphology by dissolutions of cementitious compounds around surface matrix [49, 50].

Summary and Conclusions

The present study proposes to utilize the envirosafe alkali-activated binder (AAB) incorporating fly ash and slag, which serves the dual benefit of reducing traditional-based

cementitious binders and preventing the disposal of fly ash/slag. Usage of low-carbon-emission binders is an alternate technique to upgrade the geomechanical characteristics and aid to maintain the green-sustainable environment in an economical and efficient way. The main conclusions that can be drawn from this study are as follows.

- Microanalysis results confirm the formation of new crystalline phases in AAB-treated BCS. In addition, it is also observed that the physical surface morphology of fiber–AAB-treated BCS acts as bridge network by holding the clay particles strongly around the fiber.
- Fiber-reinforced-AAB-treated BCS micrograph shows the strong interfacial surface interaction between the fiber and soil matrix. The bridge effect of fiber can efficiently change the soil brittle behavior to ductile with sufficient friction and bonding.
- The geoengineering results show that the fiber–AAB-treated BCS shows a significant improvement in tensile and shear strength behavior through interfacial friction between fiber and soil matrix.
- The tensile strength and CBR of AAB-treated soil increased by around 63.1 and 52.6% as the fiber content increased from 0 to 0.4%, and fiber reinforcement benefit attributes toward the formation of elongation than breakage.
- It is observed that the high volumetric instability of BCS can be controlled by forming a strong bond between clay mineral and cementitious products around the fiber surface. It is found that the void ratio and swelling pressure of fiber–AAB-treated soil reduced by 33% and 45%, respectively.
- Strength bearing properties in terms of CBR and UCS values of fiber–AAB-treated BCS enhance by replacing 30% fly ash with GGBS in the AAB compound up to 0.3% of fiber.
- The proposed fly ash/slag-based alkali-activated binder can be utilized practically for stabilization effectively, giving a way for avoiding traditionally based binders by contributing to maintaining the safe and eco-friendly environment.

Acknowledgements The authors would like to express their sincere gratitude to the Central Analytical Laboratory Facilities at BITS-Pilani, Hyderabad Campus, for providing the setup for the XRD, FTIR, and SEM–EDS analyses.

References

1. L.W. Ackroyd, R. Husain, Géotechnique **36**, 113 (2009)
2. B. M. Das, Chemical and Mechanical Stabilisation, Transp. Res. Board (2003)
3. P.V. Sivapullaiah, B.G. Prasad, M.M. Allam, Soil Sediment Contam. **18**, 121 (2009)
4. H. Zhao, L. Ge, T.M. Petry, Y.Z. Sun, KSCE J. Civ. Eng. **18**, 1009 (2014)
5. N. Ural, Road Mater. Pavement Des. **17**, 104 (2016)
6. S. Pourakbar, A. Asadi, B.B.K. Huat, M.H. Fasihnikoutalab, Transp. Geotech. **3**, 24 (2015)
7. S. Rios, N. Cristelo, A. Viana da Fonseca, C. Ferreira, J. Mater. Civ. Eng. **28**, 04015125 (2015)
8. F.G. Bell, Eng. Geol. **42**, 223 (1996)
9. E. Gartner, Cem. Concr. Res. **34**, 1489 (2004)
10. A. Kar, I. Ray, U.B. Halabe, A. Unnikrishnan, B. Dawson-andoh, Int, J. Cocr. Struct. Mater. **8**, 213 (2014)
11. R.P. Shukla, N.S. Parihar, J. Inst. Eng. Ser. A **97**, 299 (2016)
12. S. Miao, C. Wei, X. Huang, Z. Shen, X. Wang, F. Luo, J. Mater. Civ. Eng. **29**, 04017170 (2017)
13. G.A. Miller, S. Azad, Constr. Build. Mater. **14**, 89 (2000)
14. C. Tang, B. Shi, W. Gao, F. Chen, Y. Cai, Geotext. Geomembranes **25**, 194 (2007)
15. J. Davidovits, Alkaline Cements and Concretes, Kiev, Ukraine 1–18 (1994)
16. B. Tian, L. Ying, N. Kaimin, L. Sili, X. Jinde, L. Xinjun, J. Mater. Civ. Eng. **26**, 233 (2014)
17. T. Yetimoglu, M. Inanir, O.E. Inanir, Geotext. Geomembr. **23**, 174 (2005)
18. S.P.K. Kodicherla, D.K. Nandyala, Int. J. Geo-Eng. **10**, 1 (2019)
19. M. Ding, F. Zhang, X. Ling, B. Lin, Cold Reg. Sci. Technol. **154**, 155 (2018)
20. M. Mirzababaei, A. Arulrajah, S. Horpibulsuk, A. Soltani, N. Khayat, Geotext. Geomembr. **46**, 646 (2018)
21. B. Mishra, M. Kumar Gupta, Constr. Build. Mater. **190**, 95 (2018)
22. A. Pekrioglu Balkis, Constr. Build. Mater. **134**, 556 (2017)
23. S. Pourakbar, A. Asadi, B.B.K. Huat, M.H. Fasihnikoutalab, Environ. Geotech. **2**, 359 (2015)
24. A. Asadi, B.B.K. Huat, N. Cristelo, S. Pourakbar, M.H. Fasihnikoutalab, J. Mater. Civ. Eng. **29**, 04016206 (2016)
25. Y. Cai, B. Shi, C.W.W. Ng, C. Sheng TAng, Eng. Geol. **87**, 230 (2006)
26. A.A.S. Correia, P.J. Venda Oliveira, D.G. Custódio, Geotext. Geomembr. **43**, 97 (2015)
27. B.V.S. Viswanadham, B.R. Phanikumar, R.V. Mukherjee, Geotext. Geomembr **27**, 73 (2009)
28. A. Arulrajah, Y.-S. Xu, D.-W. Hou, M. Chen, S.-L. Shen, H.-N. Wu, Geotext. Geomembr. **43**, 515 (2015)
29. C. S. Tang, B. Shi, Y. J. Cui, C. Liu, and K. Gu, Can. Geotech. J., **49**, 1088–1101 (2012)
30. C.-S. Tang, B. Shi, J. Li, D.-Y. Wang, Y.-J. Cui, J. Mater. Civ. Eng. **28**, 04016031 (2016)
31. S. Gupta, A. GuhaRay, A. Kar, V.P. Komaravolu, Int. J. Geotech. Eng. (2018). https://doi.org/10.1080/19386362.2018.1464272
32. S. Mazhar, A. Guharay, A. Kar, G.S.S. Avinash, and R. Sirupa, *Proceedings of China-Europe Conference on Geotechnical Engineering* (Springer International Publishing, 2018)
33. A.O. Ogundalu, G.L. Oyekan, Int. J. Eng. Technol. **4**, 345 (2014)
34. S.A. Bernal, J.L. Provis, V. Rose, R. Mejía De Gutierrez, Cem. Concr. Compos. **33**, 46 (2011)
35. D.C. Sekhar, S. Nayak, Int. J. Geotech. Eng. **6362**, 1 (2017)
36. A.F. Plante, J.M. Fernández, J. Leifeld, Geoderma **153**, 1 (2009)
37. W.G. Holtz, ASTM **D121**, 641 (1954)
38. Cornell University, *Final Report on Soil Solidification Research.Ithaca, New York* (1951)
39. A. Sridharan, P. Keshavamurthy, INAEL **1**, 29–33 (2016)
40. A.K. Mishra, A. Sridharan, Int. J. Geotech. Eng. 1 (2017). https://doi.org/10.1080/19386362.2017.1405541
41. B.R. Phanikumar, R. Singla, Soils Found. **56**, 138 (2016)
42. A.A.B. Moghal, B.C.S. Chittoori, B.M. Basha, A.M. Al-Mahbashi, Int. J. Geotech. Eng. **12**, 462 (2018)

43. W.A.M. Ogila, Environ. Earth Sci. **75**, 1 (2016)
44. S. Saride, A.J. Puppala, S.R. Chikyala, Appl. Clay Sci. **85**, 39 (2013)
45. A.K. Sharma, P.V. Sivapullaiah, Soils Found. **56**, 205 (2016)
46. S.K. Vindula, R.V.P. Chavali, P.H.P. Reddy, T. Srinivas, Int. J. Geotech. Eng. **6362**, 1 (2017)
47. A.A.B. Moghal, B.C.S. Chittoori, B.M. Basha, M.A. Al-Shamrani, J. Mater. Civ. Eng. **29**, 04017014 (2017)
48. C.A. Anagnostopoulos, Appl. Clay Sci. **114**, 517 (2015)
49. V. Malik, A. Priyadarshee, Int. J. Geotech. Eng. **12**, 413 (2018)
50. A.A.B. Moghal, B.C.S. Chittoori, B.M. Basha, Road Mater. Pavement Des. **19**, 690 (2018)